Chapter 6
Fully Eulerian Formulation for Fluid-structure Interactions

This chapter is devoted to an alternative monolithic formulation for fluid-structure interactions. While the ALE scheme was based on a mapping of the Eulerian fluid system $\mathcal{F}(t)$ onto a fixed reference framework $\hat{\mathcal{F}}$ to be coupled with the Lagrangian solid domain, the Fully Eulerian formulation goes the other way around. Both problems, fluid as well as solid are modeled on the moving Eulerian domains $\mathcal{F}(t)$ and $\mathcal{S}(t)$ connected by the moving interface $\mathcal{I}(t)$. The general approach is comparable. Both subproblems can be variationally coupled such that we arrive at a monolithic global system. A conceptual difference is in the kind of interface treatment. While the ALE interface $\hat{\mathcal{I}}$ is temporally fixed, the Eulerian interface $\mathcal{I}(t)$ is moving in time and depends on the solution. The domain motion is not any longer hidden in the artificial deformation variable $\mathbf{u}_f$ but must be separately captured by the discretization. Here, we describe this rather new formulation that has been introduced by Dunne in 2006 [126, 127]. A very similar approach has been introduced by Cottet, Maitre and Milcent at about the same time [103–105]. Since then, similar approaches have been published [105, 179, 278, 282, 285, 345]. The underlying principle for all Eulerian formulations is to avoid the introduction of artificial coordinate systems that can cause a break down of the coupled scheme. In ALE formulations, the fluid's reference domain does not have a physical significance. As seen in Sect. 5.3.5 the construction of the ALE map is—up to certain degree—arbitrary. Picking the wrong map can result in a loss of regularity or invertibility and finally to a breakdown of the scheme. A Lagrangian-Eulerian mapping of the solid problem however is completely physical. Both formulations are equivalent, as long as material rupture or material overlapping is not allowed. However large the deformation or motion of the solid is, the Eulerian system will be well-posed.

Most of the recent progress that has been made with regard to the Fully Eulerian formulation is due to the intense work of Frei [153, 158, 284]. A good overview is found in [151, 154]. Finally, the last chapter of this book is a guest article by Stefan

T. Richter, *Fluid-structure Interactions*, Lecture Notes in Computational Science and Engineering 118, DOI 10.1007/978-3-319-63970-3_6

Frei and presents modern numerical techniques for simulations in the Fully Eulerian formulation, see Chap. 12.

6.1 Eulerian Models for Fluid-structure Interactions

The success of the ALE formulation for fluid-structure interactions crucially depends on the quality of the fluid domain map $\hat{T}_f$. If this mapping looses its regularity, equivalence between the variational ALE formulation in Lemma 3.11 and the classical formulations of the fluid-structure interaction problem in equation (3.4) will not hold any more. Further, we have seen that bounds on $\hat{\nabla}\hat{T}_f$ and $\nabla\hat{T}_f^{-1}$ will enter basic inequalities like the trace inequality, Poincaré inequality and also the inf-sup inequality. Even if the derivatives of $\hat{T}_f$ and $\hat{T}_f^{-1}$ are bound, the constants that will finally enter stability and error estimates can be very large.

Some configurations will necessarily lead to a degeneration of the ALE mapping. The most prominent example is given for contact problems, as a C^1-diffeomorphism between two domains with different topology cannot exist. In this section, we will introduce an alternative variational formulation for the coupled fluid-structure interaction problem that goes the opposite way: instead of mapping the moving fluid domain onto a fixed reference domain $\hat{T}_f(t) : \hat{\mathcal{F}} \to \mathcal{F}(t)$ we use an inverse map to transform the Lagrangian solid reference domain onto the Eulerian moving solid domain $\hat{T}_s(t) : \hat{\mathcal{S}} \to \mathcal{S}(t)$. Like the ALE map $\hat{T}_f$, this transformation is defined by the deformation $\hat{\mathbf{u}}_s$

$$\hat{T}_s(\hat{x}, t) := \hat{x} + \hat{\mathbf{u}}_s(\hat{x}, t).$$

There is one fundamental difference between $\hat{T}_s$ and $\hat{T}_f$. While the ALE map $\hat{T}_f$ is arbitrary and $\hat{\mathcal{F}}$ does not play a physical role, the solid domain map $\hat{T}_s$ is given by physical principles. It maps between Lagrangian and Eulerian coordinates. If the solid problem is well-posed, both formulations are valid and it holds that

1. the mapping $\hat{T}_s$ is a bijection between $\hat{\mathcal{S}}$ and $\mathcal{S}(t)$,
2. mapping $\hat{T}_s$ and inverse $\hat{T}_s^{-1}$ are differentiable,
3. the determinants $\hat{J}_s := \det(\hat{\nabla}\hat{T}_s)$ and $\hat{J}_s^{-1} = \det(\nabla\hat{T}_s^{-1})$ satisfy

$$0 < c_1 \leq \hat{J}_s \leq c_2 < \infty.$$

The well-posedness of an Eulerian formulation for fluid-structure interactions is obvious, since the Eulerian coordinates are the physical coordinates where the governing equations (the conservation laws) have been derived. The transition to the Lagrangian reference system was mainly for practical reasons, as deformation stresses can best be described in a particle centered framework. For structure mechanics both viewpoints, the Lagrangian and the Eulerian are physically relevant and the mapping between them is simply given by the deformation $\mathbf{u}$.

6.1.1 Elastic Structures in Eulerian Coordinates

In Sect. 2.1.6, we derived the basic conservation principles for moving volumes that where based on conservation of mass, momentum and angular momentum. Here, we will derive the Eulerian formulation for the structure problem on the moving solid domain $\mathcal{S}(t)$ that is given by the Lagrangian deformation of $\hat{\mathcal{S}}$

$$\mathcal{S}(t) = \{\hat{x} + \hat{\mathbf{u}}_s(\hat{x}, t),\ \hat{x} \in \hat{\mathcal{S}}\}.$$

By mass and momentum conservation, we derived the non-conservative formulation of the momentum equation (2.14)

$$\rho_s \partial_t \mathbf{v}_s + \rho_s \mathbf{v}_s \cdot \nabla \mathbf{v}_s - \nabla \cdot \boldsymbol{\sigma}_s = \rho_s \mathbf{f} \text{ in } \mathcal{S}(t),$$

where $\rho_s(x, t)$ is the Eulerian density of the solid at time t in point $x \in \mathcal{S}(t)$, $\mathbf{v}_s(x, t)$ is the Eulerian velocity and $\boldsymbol{\sigma}_s$ the Eulerian Cauchy-Stress tensor of the solid problem, also given in the Eulerian coordinate system. Here, it is necessary to remember that the transformation to Lagrangian or to an arbitrary reference system in ALE coordinates only touches the domain $\mathcal{S}(t)$ and $\hat{\mathcal{S}}$, not the image, e.g. it holds

$$\mathbf{v}(x, t) = \hat{\mathbf{v}}(\hat{x}, t),$$

for a pair $x = \hat{T}(\hat{x}, t)$. For defining a Eulerian representation $\boldsymbol{\sigma}_s$ of the Cauchy stress tensor, we must introduce a Eulerian counterpart $\mathbf{u}_s$ of the Lagrangian deformation $\hat{\mathbf{u}}_s$. We define

$$\mathbf{u}_s(x, t) = \hat{\mathbf{u}}_s(\hat{x}, t),$$

for a point $x = \hat{x} + \hat{\mathbf{u}}_s(\hat{x}, t)$. Then, it holds

$$\hat{x} = x - \hat{\mathbf{u}}_s(\hat{x}, t) = x - \mathbf{u}_s(x, t),$$

which defines the inverse mapping $T_s(t) : \mathcal{S}(t) \to \hat{\mathcal{S}}$

$$T_s(x, t) := x - \mathbf{u}_s(x, t), \quad T_s = \hat{T}_s^{-1}.$$

Further, considering Lemma 2.9 and (3.28), it holds

$$T_s \circ \hat{T}_s = \mathrm{id} \quad \Rightarrow \quad \nabla T_s =: \mathbf{F}_s = \hat{\mathbf{F}}_s^{-1} = (\hat{\nabla} \hat{T}_s)^{-1}, \quad J_s = \hat{J}_s^{-1}. \tag{6.1}$$

And with $\hat{T}_s := \hat{x} + \hat{\mathbf{u}}_s$ and $T_s := x - \mathbf{u}_s$ it finally follows that

$$[I - \nabla \mathbf{u}_s] = [I + \hat{\nabla} \hat{\mathbf{u}}_s]^{-1} \quad \Leftrightarrow \quad \nabla \mathbf{u}_s = I - [I + \hat{\nabla} \hat{\mathbf{u}}_s]^{-1} = I - \hat{\mathbf{F}}_s^{-1}.$$

Using these relations, we can transform the Cauchy stress tensor $\hat{\boldsymbol{\sigma}}_s$ from Lagrangian to Eulerian coordinates.

Lemma 6.1 (Cauchy Stress Tensor for the St. Venant Kirchhoff Material in Eulerian Coordinates) *The Cauchy stress tensor of the St. Venant Kirchhoff material in Eulerian coordinates is given by*

$$\boldsymbol{\sigma}_s = J_s \mathbf{F}_s^{-1} \left(2\mu \mathbf{E}_s + \lambda_s \operatorname{tr}(\mathbf{E}_s) I\right) \mathbf{F}_s^{-T}, \quad \mathbf{E}_s := \frac{1}{2}\left(\mathbf{F}_s^{-T}\mathbf{F}_s^{-1} - I\right).$$

Proof The second Piola Kirchhoff stress tensor $\hat{\boldsymbol{\Sigma}}_s$ of the St. Venant Kirchhoff material was introduced in Definition 2.18 as

$$\hat{\boldsymbol{\Sigma}}_s = 2\mu_s \hat{\mathbf{E}}_s + \lambda_s \operatorname{tr}(\hat{\mathbf{E}}_s) I$$

with the Green-Lagrangian strain tensor

$$\hat{\mathbf{E}}_s := \frac{1}{2}(\hat{\mathbf{F}}_s^T \hat{\mathbf{F}}_s - I).$$

The relation between Cauchy stress tensor and 2nd Piola Kirchhoff stress tensor is given by the Piola transformation, see Definition 2.13:

$$\hat{\boldsymbol{\sigma}}_s = \hat{J}_s^{-1} \hat{\mathbf{F}}_s \hat{\boldsymbol{\Sigma}}_s \hat{\mathbf{F}}_s^T$$

Then, by (6.1) we get the its Eulerian representation as

$$\boldsymbol{\sigma}_s = J_s \mathbf{F}_s^{-1} \boldsymbol{\Sigma}_s \mathbf{F}_s^{-T},$$

with the 2nd Piola Kirchhoff tensor expressed in Eulerian coordinates

$$\boldsymbol{\Sigma}_s = 2\mu_s \mathbf{E}_s + \lambda_s \operatorname{tr}(\mathbf{E}_s) I.$$

The Eulerian Green-Lagrangian strain tensor is given by

$$\mathbf{E}_s := \frac{1}{2}(\mathbf{F}_s^{-T}\mathbf{F}_s^{-1} - I).$$

□

The derivation of the Cauchy stress tensor $\boldsymbol{\sigma}_s$ in Eulerian coordinates completes the description of the momentum equation. It remains to add an equation for the unknown Eulerian density ρ_s. By defining

$$\rho_s(x,t) = \hat{\rho}_s(\hat{x},t),$$

and using (2.27), it holds

$$\rho_s(x,t) = J_s \hat{\rho}_s^0(\hat{x}), \tag{6.2}$$

where $\hat{\rho}_s^0$ is the density of the solid at time $t = 0$ in the corresponding reference coordinate. Usually one considers homogenous materials, such that relation (6.2) simplifies to

$$\rho_s(x,t) = J_s \hat{\rho}_s^0. \tag{6.3}$$

In the Eulerian coordinate framework, we must also transform the relation between deformation and velocity, compare Lemma 2.10:

$$d_t \hat{\mathbf{u}}_s = \partial_t \mathbf{u}_s + \mathbf{v}_s \cdot \nabla \mathbf{u}_s, \quad d_t \hat{\mathbf{v}}_s = \partial_t \mathbf{v}_s + \mathbf{v}_s \cdot \nabla \mathbf{v}_s.$$

Combining the foregoing discussion we define:

Problem 6.2 (Solid Problem in Eulerian Coordinates) *The elastic deformation of a St. Venant Kirchhoff material in Eulerian coordinates is given by*

$$J_s \hat{\rho}_s (\partial_t \mathbf{v}_s + \mathbf{v}_s \cdot \nabla \mathbf{v}_s) - \nabla \cdot \boldsymbol{\sigma}_s = J_s \hat{\rho}_s \mathbf{f}, \quad \partial_t \mathbf{u}_s + \mathbf{v}_s \cdot \nabla \mathbf{u}_s = \mathbf{v}_s,$$

with the Eulerian formulation of the Cauchy stress tensor

$$\boldsymbol{\sigma}_s := J_s \mathbf{F}_s^{-1} (2\mu_s \mathbf{E}_s + \lambda_s \operatorname{tr}(\mathbf{E}_s) I) \mathbf{F}_s^{-T}, \quad \mathbf{E}_s := \frac{1}{2} \left(\mathbf{F}_s^{-T} \mathbf{F}_s^{-1} - I \right),$$

and the Eulerian deformation gradient

$$\mathbf{F}_s = I - \nabla \mathbf{u}_s.$$

In [151, 154] a derivation of the fluid-structure interaction problem in Eulerian coordinates is given without prior introduction of the Lagrangian problems.

Apart from the complex nonlinear form of the stress tensor, the solid problem is naturally given in Eulerian coordinates. The immediate drawback of this Eulerian formulation is twofold:

- The problem is formulated on the moving domain $\mathcal{S}(t)$ that is a priori unknown and part of the solution. For defining a standard variational formulation of the solid equation in Eulerian coordinates, all difficulties already discussed in Sect. 2.5 must be tackled again.
- By transformation to Eulerian coordinate, convective terms are introduced:

$$d_t \hat{\mathbf{v}} = \partial_t \mathbf{v} + \mathbf{v} \cdot \nabla \mathbf{v}, \quad d_t \hat{\mathbf{u}} = \partial_t \mathbf{u} + \mathbf{v} \cdot \nabla \mathbf{u}.$$

A discretization of this convective term will cause numerical stability problems, as known for the transport term in the Navier-Stokes equations. Numerical methods must introduce artificial stabilization terms that will cause loss of conservation principles.

Finally, we introduce a variational formulation of the structure problem in Eulerian coordinates, derived by multiplication with suitable test functions. Find

$$\{\mathbf{v}_s, \mathbf{u}_s\} \in \mathcal{V}_s(t) \times \mathcal{W}_s(t),$$

such that

$$\begin{aligned} \left(J_s\hat{\rho}_s(\partial_t\mathbf{v}_s + \mathbf{v}_s\cdot\nabla\mathbf{v}_s), \phi_s\right)_{\mathcal{S}(t)} & \\ +\left(\boldsymbol{\sigma}_s, \nabla\phi_s\right)_{\mathcal{S}(t)} &= \left(J_s\hat{\rho}_s^0\mathbf{f}, \phi\right)_{\mathcal{S}(t)} \quad \forall\phi_s \in \mathcal{V}_s^{\text{test}} \\ \left(\partial_t\mathbf{u}_s + \mathbf{v}_s\cdot\nabla\mathbf{u}_s - \mathbf{v}_s, \psi_s\right)_{\mathcal{S}(t)} &= 0 \quad \forall\psi_s \in \mathcal{W}_s^{\text{test}}, \end{aligned} \tag{6.4}$$

While the Lagrangian velocity $\hat{\mathbf{v}}_s \in L^2(\hat{\mathcal{S}})^d$ is defined as L^2-projection the Eulerian counterpart requires some control over the derivative in direction of $\mathbf{v}_s$.

6.1.2 Fluid-structure Interaction in Eulerian Coordinates

With the variational formulation of the Eulerian structure problem shown in (6.4) it is straightforward to formulate the coupled fluid-structure interaction problem in Eulerian coordinates. We simple combine (6.4) with the incompressible Navier-Stokes equations (2.48) on the moving domain $\mathcal{F}(t)$ by adding appropriate interface conditions

$$\begin{aligned} (\rho_f(\partial_t\mathbf{v}_f + \mathbf{v}_f\cdot\nabla\mathbf{v}_f), \phi_f)_{\mathcal{F}(t)} + (\boldsymbol{\sigma}_f, \nabla\phi_f)_{\mathcal{F}(t)} &= (\rho_f\mathbf{f}, \phi_f)_{\mathcal{F}(t)} \\ (\nabla\cdot\mathbf{v}_f, \xi_f)_{\mathcal{F}(t)} &= 0 \\ (J_s\hat{\rho}_s(\partial_t\mathbf{v}_s + \mathbf{v}_s\cdot\nabla\mathbf{v}_s), \phi_s)_{\mathcal{S}(t)} + (\boldsymbol{\sigma}_s, \nabla\phi_s)_{\mathcal{S}(t)} &= (J_s\hat{\rho}_s^0\mathbf{f}, \phi)_{\mathcal{S}(t)} \\ (\partial_t\mathbf{u}_s + \mathbf{v}_s\cdot\nabla\mathbf{u}_s - \mathbf{v}_s, \psi_s)_{\mathcal{S}(t)} &= 0 \\ \mathbf{v}_f &= \mathbf{v}_s \quad \text{on } \mathcal{I}(t), \\ \boldsymbol{\sigma}_f n &= \boldsymbol{\sigma}_s\mathbf{n} \quad \text{on } \mathcal{I}(t) \end{aligned} \tag{6.5}$$

Variational coupling of these equations on $\mathcal{F}(t)$ and $\mathcal{S}(t)$ is easily possible following the guidelines introduced in Sect. 3.4. As the two domain $\mathcal{F}(t)$ and $\mathcal{S}(t)$ match and share a common interface $\mathcal{I}(t) = \partial\mathcal{F}(t) \cap \partial\mathcal{S}(t)$, we can combine the trial space to embed continuity of velocities into the variational formulation

$$\mathbf{v} \in \mathcal{V} = H_0^1(\Omega)^d, \quad \mathbf{v}_f = \mathbf{v}\big|_{\mathcal{F}(t)}, \quad \mathbf{v}_s = \mathbf{v}\big|_{\mathcal{S}(t)}.$$

For realizing the dynamic coupling condition, we combine the test spaces of the momentum equations:

$$\phi \in \mathcal{V} = H_0^1(\Omega)^d, \quad \phi_f = \phi\big|_{\mathcal{F}(t)}, \quad \phi_s = \phi\big|_{\mathcal{S}(t)}.$$

We can define the variational formulation of the Fully Eulerian fluid-structure interaction problem:

Problem 6.3 (Variational Formulation of the Eulerian Fluid-structure Interaction Problem) *Let*

$$\mathbf{v} \in \mathcal{V} = H_0^1(\Omega)^d,\ p_f \in L^2(\mathcal{F}(t)),\ \mathbf{u}_s \in H_0^1(\Omega)^d,$$

be the solution of the variational problem

$$\begin{aligned}
&(\rho_f(\partial_t \mathbf{v}_f + \mathbf{v}_f \cdot \nabla \mathbf{v}_f), \phi)_{\mathcal{F}(t)} + (\boldsymbol{\sigma}_f, \nabla\phi)_{\mathcal{F}(t)} \\
&\quad + (J_s\hat{\rho}_s(\partial_t \mathbf{v}_s + \mathbf{v}_s \cdot \nabla \mathbf{v}_s), \phi)_{\mathcal{S}(t)} + (\boldsymbol{\sigma}_s, \nabla\phi)_{\mathcal{S}(t)} = (\rho_f \mathbf{f}, \phi)_{\mathcal{F}(t)} \\
&\qquad\qquad + (J_s\hat{\rho}_s^0 \mathbf{f}, \phi)_{\mathcal{S}(t)} \qquad (6.6)\\
&(\nabla \cdot \mathbf{v}_f, \xi_f)_{\mathcal{F}(t)} = 0 \\
&(\partial_t \mathbf{u}_s + \mathbf{v}_s \cdot \nabla \mathbf{u}_s - \mathbf{v}_s, \psi_s)_{\mathcal{S}(t)} = 0,
\end{aligned}$$

for all

$$\phi \in \mathcal{V},\ \xi_f \in L^2(\mathcal{F}(t)),\ \psi_s \in L^2(\mathcal{S}(t))^d.$$

Given sufficient regularity, a transformation of $\{\mathbf{v}, p_f, \mathbf{u}_s\}$ *to Lagrangian coordinates (in the solid domain) also solves the fluid-structure interaction problem in classical formulation (3.4).*

Apparently, the Eulerian formulation of the fluid-structure interaction problem has a simpler structure than the ALE formulation. No mapping, at least no artificial mapping between domains is necessary. Hence, there is no obvious reason why the Eulerian formulation should show limits when treating problems with very large deformation, motion or even contact. All this is true, the simplicity of the variational formulation in Problem 6.3 however hides one essential vagueness. The deformation of the domains $\mathcal{F}(t)$ and $\mathcal{S}(t)$ is given by the solution, to be precise, by the deformation of the solid domain

$$\mathrm{id} + \hat{\mathbf{u}}_s : \hat{\mathcal{S}} \to \mathcal{S}(t).$$

The formulation in Eulerian coordinates is based on the inverse of this relation:

$$\mathrm{id} - \mathbf{u}_s : \mathcal{S}(t) \to \hat{\mathcal{S}},$$

the so-called *backward characteristic*. The complete derivation of the Eulerian method hides out one dilemma, that is inherent to fluid-structure interaction problems. The domains $\mathcal{F}(t)$ and $\mathcal{S}(t)$ are moving and depend on the solution. However, for assembling the Eulerian formulation (6.6), we must—for every point $x \in \Omega$—know its affiliation to the fluid-domain $x \in \mathcal{F}(t) \subset \Omega$ or solid domain $x \in \mathcal{S}(t) \subset \Omega$. This appears to be an irreconcilable barrier for implicit monolithic formulations of the Eulerian model, as the domain affiliation is prerequisite for setting up the equations, whose solution is required for defining the affiliation. The next section will describe techniques for capturing the moving interface.

6.2 Interface Capturing and the Initial Point Set Method

To work around this dilemma, we need to enrich the system of equations by variables used to capture the location of the two domains. Multi-phase methods that live on a fixed background system and where the interface between the phases in freely moving are called *interface-capturing* techniques. One of the most prominent *interface-capturing* methods is the *Level-Set method* by Osher [257] and Sethian [307].

Remark 6.4 (Level-Sets) Assume that $\mathcal{F}(0) \cup \mathcal{I}(0) \cup \mathcal{S}(0)$ is the initial partitioning of the domain. We define a level-set function $\Psi(x, 0)$ as the signed distance function belonging to this partitioning

$$\Psi(x,0) := \begin{cases} \operatorname{dist}(x, \mathcal{I}(0)) & x \in \mathcal{S}(0), \\ 0 & x \in \mathcal{I}(0), \\ -\operatorname{dist}(x, \mathcal{I}(0)) & x \in \mathcal{F}(0). \end{cases}$$

We assume that the domain-partitioning is moving with a velocity field $\mathbf{v}$. Then, the level-set function is advected with this field by

$$\frac{\partial \Psi}{\partial t} + \mathbf{v} \cdot \nabla \Psi = 0,$$

or, if motion is restricted to the normal direction by

$$\frac{\partial \Psi}{\partial t} + v_n |\nabla \Psi| = 0,$$

where $v_n = \mathbf{v} \cdot \mathbf{n}$ is the velocity in normal direction. This allows for a level set representation of the interface

$$\mathcal{I}(t) = \{x \in \mathbb{R}^d,\ \Psi(x,t) = 0\}.$$

Normal vectors and curvatures can be calculated based on the level set function. Some problems of level set formulations is the need of reinitialization if distances are to be discovered. An auxiliary equation is introduced at time t' to normalize the gradient $\nabla\Psi$ to one, e.g. by

$$\partial_\tau \Psi + \operatorname{sgn}(\Psi(t'))\,(|\nabla\Psi| - 1) = 0, \quad \tau > 0.$$

Numerical schemes for the advection of the level set function will introduce diffusion. This will cause a smearing of sharp corners, that cannot be well approximated as zero lines of level sets. Nevertheless, level sets are one of the most established methods for capturing interfaces in Eulerian based simulations, see [257, 307].

One of the disadvantages connected to the Level-Set method is a degeneration of edges. Due to numerical dissipation and due to the reinitialization procedure, edges will be smoothened. While this does not pose a major problem for multiphase flows, where the interface usually does not show edges, the conservation of sharp edges (e.g. of the solid subdomain) is crucial in fluid-structure interaction applications. He and Qiao introduced a Eulerian formulation for fluid-structure interactions, where the interface was captured with the help of three Level-Set functions [179].

Here, we describe the *Initial Point Set method* for capturing the interface between fluid- and solid-domain. To be precise: instead of capturing the interface location, we will capture the complete reference coordinate system. We know that at time $t \geq 0$, a spatial coordinate $x \in \Omega$ belongs to the solid domain $x \in \mathcal{S}(t)$, if it holds

$$T_s(x,t) = \hat{x} - \mathbf{u}_s(x,t) \in \hat{\mathcal{S}},$$

if the coordinate $x \in \Omega$ is the location of the particle $\hat{x} \in \hat{\mathcal{S}}$ at time t. This construction will be transferred to the fluid-domain. Assume that $\mathbf{u}_f(x,t)$ is a vector field, such that:

$$x - \mathbf{u}_f(x,t) \in \hat{\mathcal{F}} \quad \Leftrightarrow \quad x \in \mathcal{F}(t).$$

By $\mathbf{u}_f$ we denote the Eulerian deformation of the fluid-domain. Similar to the fluid domain map $\hat{\mathbf{u}}_f$ in the ALE formulation, this deformation $\mathbf{u}_f$ does not describe the physical motion of a particle. We use $\mathbf{u}_f$ to define the inverse fluid-map $T_f(x,t) = x - \mathbf{u}_f(x,t)$. Next, we assume that there is a continuous transition from T_f to T_s on the interface $\mathcal{I}(t)$. Then, we can define one global inverse mapping

$$T(x,t) := \begin{cases} T_s(x,t) & x \in \mathcal{S}(t) \\ T_s(x,t) = T_f(x,t) & x \in \mathcal{I}(t) \\ T_f(x,t) & x \in \mathcal{F}(t). \end{cases}$$

Based on this mapping, we can decide the domain affiliation for every spatial coordinate $x \in \Omega$

$$x \in \mathcal{S}(t) \Leftrightarrow T(x,t) \in \hat{\mathcal{S}},$$
$$x \in \mathcal{F}(t) \Leftrightarrow T(x,t) \in \hat{\mathcal{F}}.$$

This inverse map $T(x,t)$ is exactly the *backward-characteristic* $Y(x,t)$ used in the formulations of Cottet, Milcent and Maitre [105, 242].

It remains to define the Eulerian fluid-domain deformation $\mathbf{u}_f$ in an implicit way. To derive a continuous transition between T_f and T_s, the deformations $\mathbf{u}_f$ and $\mathbf{u}_s$ will need to be continuous. We can define $\mathbf{u}_f$ simply by an extension of $\mathbf{u}_s$ to $\mathcal{F}(t)$.

Remark 6.5 (Initial Point Set) This construction looks very similar to the construction of the ALE-map in the context of the Arbitrary Lagrangian Eulerian model and one could argue that the same difficulties are introduced. As we define an arbitrary extension $\mathbf{u}_f$ of the solid's deformation $\mathbf{u}_s$, numerical artifacts come into place. There are however two fundamental differences: first, the inverse map $T(x,t)$ inside the fluid domain is not used for any kind of mapping. We do not require its inverse or its derivatives. Instead, it is for look-up purposes only. Second, we do not even require that $T_f(x,t) \in \hat{\mathcal{F}}$ for $x \in FL(t)$. It is completely sufficient that $x \in \mathcal{F}(t)$ is mapped outside of the solid domain. Therefore, we can relax the definition of the extension $\mathbf{u}_f$, i.e. by requiring Dirichlet values only on the interface and by relaxing the look-up property. Instead of requiring $T(x,t) \in \hat{\mathcal{F}}$ for $x \in \mathcal{F}(t)$, we simply demand $T(x,t) \notin \hat{\mathcal{S}}$ for such fluid points.

Definition 6.6 (Initial Point Set) A vector field $\Phi_{\text{IPS}} \in C(I; C(\Omega))$ is called Initial Point Set, if for $x \in \Omega$ and $t \geq 0$ it holds

$$\Phi_{\text{IPS}}(x,t) = x - \mathbf{u}_s(x,t) \in \hat{\mathcal{S}} \quad \Rightarrow \quad x \in \mathcal{S}(t)$$
$$\Phi_{\text{IPS}}(x,t) \notin \hat{\mathcal{S}} \quad \Rightarrow \quad x \in \mathcal{F}(t)$$

Within the solid domain, the vector field Φ_{IPS} is called the *backward characteristic* [105]. Finally, we can indicate possibilities for the construction of $\mathbf{u}_f$. One simple option is to choose one more a harmonic extension of $\mathbf{u}_s$

$$-\Delta \mathbf{u}_f = 0 \text{ in } \mathcal{F}(t), \quad \mathbf{u}_f = \mathbf{u}_s \text{ on } \mathcal{I}(t), \quad \partial_n \mathbf{u}_f = 0 \text{ on } \partial\Omega_f(t) \setminus \mathcal{I}(t).$$

Here, we have chosen homogenous Neumann boundary conditions on the outer boundary of the fluid-domain. This deformation $\mathbf{u}_f$ will not define a mapping back to a reference domain, but as discussed, this property is not necessary. In Sect. 5.3.5 we have discussed techniques for defining the ALE map. Harmonic extension did not perform well, mostly due to singularities at edges entering the fluid domain. In the context of the Initial Point Set, this problem is smaller, as the extension must not be inverted. Finally, we can close the formulation of the coupled fluid-structure interaction problem in Eulerian coordinate.

Problem 6.7 (Initial Point Set Formulation of the Eulerian Fluid-structure Interaction Problem) *Let*

$$\mathbf{v} \in \mathcal{V} = H_0^1(\Omega)^d,\ p_f \in L^2(\mathcal{F}(t)),\ \mathbf{u}_s \in H_0^1(\Omega)^d,$$

be the solution of the variational problem

$$\begin{aligned}
&(\rho_f(\partial_t \mathbf{v} + \mathbf{v}\cdot\nabla\mathbf{v}), \phi)_{\mathcal{F}(t)} + (\boldsymbol{\sigma}_f, \nabla\phi)_{\mathcal{F}(t)} \\
&\quad + (J_s\hat{\rho}_s(\partial_t \mathbf{v} + \mathbf{v}\cdot\nabla\mathbf{v}), \phi)_{\mathcal{S}(t)} + (\boldsymbol{\sigma}_s, \nabla\phi)_{\mathcal{S}(t)} = (\rho_f \mathbf{f}, \phi)_{\mathcal{F}(t)} + (J_s\hat{\rho}_s^0 \mathbf{f}, \phi)_{\mathcal{S}(t)} \\
&\qquad\qquad (\nabla\cdot\mathbf{v}, \xi_f)_{\mathcal{F}(t)} = 0 \\
&\qquad\qquad (\partial_t \mathbf{u} + \mathbf{v}\cdot\nabla\mathbf{u} - \mathbf{v}, \psi_s)_{\mathcal{S}(t)} = 0 \\
&\qquad\qquad (\nabla\mathbf{u}, \nabla\psi_f)_{\mathcal{F}(t)} = 0
\end{aligned}$$

for all

$$\phi \in \mathcal{V}, \quad \xi_f \in L^2(\mathcal{F}(t)), \quad \psi_s \in L^2(\mathcal{S}(t))^d, \quad \psi_f \in H_0^1(\mathcal{F}(t); \mathcal{I})^d.$$

Given sufficient regularity, a transformation of $\{\mathbf{v}, p_f, \mathbf{u}_s\}$ *to Lagrangian coordinates (in the solid domain) also solves the fluid-structure interaction problem in classical formulation (3.4).*

Remark 6.8 (Eulerian FSI and Multiphase-Flows) The Fully Eulerian formulation for fluid-structure interactions is closely related to Eulerian models for multiphase flows, where one conservation law is given on a domain Ω

$$\rho(\partial_t \mathbf{v} + \mathbf{v}\cdot\nabla\mathbf{v}) - \nabla\cdot\boldsymbol{\sigma} = 0,$$

and where the material parameters, such as density or viscosity depend on the location

$$\rho(x,t) = \begin{cases} \rho_1 & x \in \mathcal{F}_1(t), \\ \rho_2 & x \in \mathcal{F}_2(t) \end{cases}.$$

The fundamental difference to fluid-structure interactions however is that only one type of differential operator is defined. In fluid-structure interactions, we have a transition from a hyperbolic equation in the solid domain to a parabolic equation in the fluid domain. This brings along the already discussed regularity problems on the interface. For multiphase flows, there exist approaches, that work with a smoothing of the parameters (density and viscosity) at the interface, such that it does not need to be sharply resolved.

By introducing the characteristic functions with respect to fluid- and solid-domain χ_f and χ_s

$$\chi_s(x,t) := \begin{cases} 1 & x - \mathbf{u}(x,t) \in \hat{\mathcal{S}}, \\ 0 & x - \mathbf{u}(x,t) \notin \hat{\mathcal{S}} \end{cases}, \quad \chi_f(x,t) := 1 - \chi_s(x,t),$$

the coupled momentum equations is shortly written as

$$\begin{aligned} \Big(\rho(\partial_t \mathbf{v} + \mathbf{v}\cdot\nabla\mathbf{v}),\phi\Big) + \Big(\boldsymbol{\sigma},\nabla\phi\Big) &= \Big(\rho\mathbf{f},\phi\Big), \\ \rho &= \chi_f\rho_f + \chi_s J_s \hat{\rho}_s, \\ \boldsymbol{\sigma} &= \chi_f\boldsymbol{\sigma}_f + \chi_s\boldsymbol{\sigma}_s. \end{aligned} \tag{6.7}$$

The introduction of such a characteristic function simplifies the formulation. The difficulties are however only hidden in a clever formulation.

6.3 Time-Discretization of the Fully Eulerian Framework

In the spirit of Sect. 4.6, the Fully Eulerian Formulation leads to an interface problem with an interface that is moving in time. A straightforward discretization of the Eulerian momentum equation (6.7) with the backward Euler method

$$\Big(\rho(k^{-1}\mathbf{v}^n + \mathbf{v}^n\cdot\nabla\mathbf{v}^n),\phi\Big) + \Big(\boldsymbol{\sigma}(\mathbf{v}^n,p^n),\nabla\phi\Big) = \Big(\rho k^{-1}\mathbf{v}^{n-1} + \rho\mathbf{f}^n,\phi\Big),$$

would result in a reduction of the convergence order, as the solution must not be differentiable in time, i.e.

$$\frac{\mathbf{v}^n(x) - \mathbf{v}^{n-1}(x)}{k},$$

may refer to a point $x \in \Omega$, which is solid $x \in \mathcal{S}(t_{n-1})$ at the old point in time and fluid $x \in \mathcal{F}(t_n)$ at the new one.

To derive a simple first order scheme, it is sufficient, to properly evaluate the projection of the old time step to the new domain partitioning. Let

$$\Omega^n = \mathcal{F}^n \cup \mathcal{I}^n \cup \mathcal{S}^n,$$

and

$$T_n : \Omega^{n-1} \to \Omega^n,$$

be given by the deformation $\mathbf{u}^n$

$$T_n(x) := x + \mathbf{u}^n(x) - \mathbf{u}^{n-1}(x), \quad T_n^{-1}(x) = x - \mathbf{u}^n(x) + \mathbf{u}^{n-1}(x).$$

With help of this mapping, which is available by the Initial Point Set method, a function $\mathbf{v}^{n-1}$ from time step t_{n-1} can be approximated on the partitioning Ω^n via

$$F(\phi) = (\rho \mathbf{f}^n, \phi) + \big((\rho \circ T_n^{-1})(\mathbf{v}^{n-1} \circ T_n^{-1}), \phi\big).$$

As T_n and so T_n^{-1} implicitly depends on the new deformation $\mathbf{u}^n$, which is unknown in a fully coupled Eulerian fluid-structure interaction setting, the evaluation of this right hand side is an implicit part of the equation.

The theoretical analysis of high order accurate time stepping methods for moving interface problems, where the interface-motion comes from the solution itself is still open. Transferring the parabolic setting from Sect. 4.6 to the Eulerian framework for fluid-structure interactions experimentally gives the correct order, see [151].

All higher order accurate schemes will require an implicit iteration on the domain partitioning, as $\Omega^n = \mathcal{F}^n \cup \mathcal{I}^n \cup \mathcal{S}^n$ is only available, when $\mathbf{u}^n$ itself is available. In a Newton like procedure, this will call for derivatives with respect to the domain motion, see the following Sect. 6.4.

To avoid such an effort, reduced order approximation could be used. In [282], non-stationary problems in the Eulerian framework have been approximated by a fully explicit treatment of the interface location, i.e. by decoupling the geometry problem from the momentum equations. Better results can be expected by using higher order extrapolations. If problems with possible contact are considered, explicit handling of the interface motion will result in restrictive time step conditions—at least, if the interface is close to contact. Such situations can efficiently be handled by means of adaptive time step control

In [284] a second order accurate time stepping scheme for parabolic interface problems is presented. A priori estimates of optimal order are shown. This scheme has been applied to the Eulerian formulation of fluid-structure interactions as presented in [151, 154]. In Chap. 12 some details on the application of this advanced time stepping schemes are presented.

6.4 Linearizations of the Fully Eulerian Coordinates

One of the benefits of an Eulerian formulation for fluid-structure interactions is the ease of the variational setting, see Problem 6.7. The complete problem is given as

$$\begin{aligned} A(U)(\Phi) =& (\rho_f(\partial_t \mathbf{v} + \mathbf{v} \cdot \nabla \mathbf{v}), \phi)_{\mathcal{F}(t)} + (\boldsymbol{\sigma}_f, \nabla \phi)_{\mathcal{F}(t)} + (\nabla \cdot \mathbf{v}, \xi_f)_{\mathcal{F}(t)} \\ &+ (J_s \hat{\rho}_s(\partial_t \mathbf{v} + \mathbf{v} \cdot \nabla \mathbf{v}), \phi)_{\mathcal{S}(t)} + (\boldsymbol{\sigma}_s, \nabla \phi)_{\mathcal{S}(t)} \\ &+ (\partial_t \mathbf{u} + \mathbf{v} \cdot \nabla \mathbf{u} - \mathbf{v}, \psi_s)_{\mathcal{S}(t)} + (\nabla \mathbf{u}, \nabla \psi_f)_{\mathcal{F}(t)}, \end{aligned} \tag{6.8}$$

with

$$\boldsymbol{\sigma}_s = J_s \mathbf{F}_s^{-1}(2\mu \mathbf{E}_s + \lambda_s \operatorname{tr}(\mathbf{E}_s) I)\mathbf{F}_s^{-T}, \quad \mathbf{E}_s = \frac{1}{2}\left(\mathbf{F}_s^{-T}\mathbf{F}_s^{-1} - I\right).$$

Most of the terms appearing in this formulation are linear or have a quadratic nonlinearity. Only the inverse deformation gradient's determinant J_s and the solid's stresses require closer attention. The characteristic difficulty will be the dependency of the integrals on the domains $\mathcal{F}(t)$ and $\mathcal{S}(t)$, which are moving in time. Hence, geometric derivatives must be considered. For the following derivation we closely follow the approach in Sect. 5.2.2, in particular Theorem 5.2 and Lemma 5.4.

Lemma 6.9 (Derivatives of the Eulerian Deformation Gradient) *Let* $\mathbf{F} = I - \nabla \mathbf{u}$, $J := \det(\mathbf{F})$ *and* $\mathbf{E} := \frac{1}{2}(\mathbf{F}^{-T}\mathbf{F}^{-1} - I)$

$$(i) \quad \frac{d\mathbf{F}}{d\mathbf{u}}(\mathbf{w}) = -\nabla \mathbf{w},$$

$$(ii) \quad \frac{d\mathbf{F}^T}{d\mathbf{u}}(\mathbf{w}) = -\nabla \mathbf{w}^T,$$

$$(iii) \quad \frac{d\mathbf{F}^{-1}}{d\mathbf{u}}(\mathbf{w}) = \mathbf{F}^{-1}\nabla \mathbf{w}\nabla \mathbf{F}^{-1},$$

$$(iv) \quad \frac{d\mathbf{F}^{-T}}{d\mathbf{u}}(\mathbf{w}) = \mathbf{F}^{-T}\nabla \mathbf{w}^T\nabla \mathbf{F}^{-T},$$

$$(v) \quad \frac{dJ(\mathbf{u})}{d\mathbf{u}}(\mathbf{w}) = -J\mathbf{F}^{-T} : \nabla \mathbf{w} = -J \operatorname{tr}(\mathbf{F}^{-1}\nabla \mathbf{w}),$$

$$(vi) \quad \frac{d\mathbf{E}(\mathbf{u})}{d\mathbf{u}}(\mathbf{w}) = \frac{1}{2}\mathbf{F}^{-T}(\nabla \mathbf{w}^T\nabla \mathbf{F}^{-T} + \mathbf{F}^{-1}\nabla \mathbf{w})\mathbf{F}^{-1}$$

Proof We note $\mathbf{F} = \hat{\mathbf{F}}^{-1}$ and refer the reader to Lemma 5.4. □

By these derivation rules most of the terms in the Jacobian of the Eulerian formulation (6.8) can be expressed.

What remains, is the handling of the formulation's dependency on the domain motion. Here, the concept of geometric derivatives, *shape calculus* must be considered. It holds

Theorem 6.10 (Directional Shape Derivatives) *Let* $\hat{\Omega} \subset \mathbb{R}^d$ *be a domain with piece-wise* C^1 *boundary,* $\hat{T}(\hat{x}) := \hat{x} + \hat{\mathbf{u}}$ *be a smooth domain map* $\hat{T} : \hat{\Omega} \to \Omega(\mathbf{u})$, *such that* $\hat{T} \in W^{1,1}(\hat{\Omega})$. *Further, let* $f \in W^{1,1}(\Omega(\mathbf{u}))$. *It holds*

$$\frac{d}{ds}\int_{\Omega(\mathbf{u}+s\mathbf{w})} f\, dx\Big|_{s=0} = \int_{\partial\Omega(\mathbf{u})} (\mathbf{n}\cdot\mathbf{w}) f\, do, \tag{6.9}$$

where $\mathbf{n}$ *is the outward facing normal vector on* $\partial\Omega(\mathbf{u})$.

Proof Let $\mathbf{u}, \mathbf{w}$ be given with Lagrangian counter-part $\hat{\mathbf{u}}(\hat{x}, t) = \mathbf{u}(x, t)$ and $\hat{\mathbf{w}}(\hat{x}, t) = \mathbf{w}(x, t)$. It holds

$$\frac{d}{ds}\int_{\Omega(\mathbf{u}+s\mathbf{w})} f \,\mathrm{d}x = \int_{\hat{\Omega}} \frac{d}{ds}\hat{J}(\hat{\mathbf{u}} + s\hat{\mathbf{w}}) f(\hat{x} + \hat{\mathbf{u}} + s\hat{\mathbf{w}}) \,\mathrm{d}\hat{x} \tag{6.10}$$

where

$$\hat{J}(\hat{\mathbf{u}} + s\hat{\mathbf{w}}) = \det\left(I + \hat{\nabla}(\hat{\mathbf{u}} + s\hat{\mathbf{w}})\right). \tag{6.11}$$

Then, by Lemma 5.4, it holds

$$\begin{aligned}\frac{d}{ds}\hat{J}(\hat{\mathbf{u}} + s\mathbf{w}) f(\hat{x} + \hat{\mathbf{u}} + s\hat{\mathbf{w}})\Big|_{s=0} \\ = \hat{J}(\hat{\mathbf{u}}) f(\hat{x} + \hat{\mathbf{u}}) \hat{\mathbf{F}}^{-T}(\mathbf{u}) : \hat{\nabla}\hat{\mathbf{w}} + \hat{J}(\hat{\mathbf{u}}) \nabla f(\hat{x} + \hat{\mathbf{u}}) \cdot \hat{\mathbf{w}}.\end{aligned}$$

Therefore, by mapping back to $\Omega(\mathbf{u})$ and with help of integration by parts:

$$\begin{aligned}\frac{d}{d\mathbf{u}}\int_{\Omega(\mathbf{u}+s\mathbf{w})} f \,\mathrm{d}x\Big|_{s=0} &= \int_{\Omega(\mathbf{u})} fI : \nabla w \,\mathrm{d}x + \int_{\Omega(\mathbf{u})} \nabla f \cdot \mathbf{w} \,\mathrm{d}x \\ &= \int_{\partial\Omega(\mathbf{u})} (\mathbf{n} \cdot \mathbf{w}) f \,\mathrm{d}x - \int_{\Omega(\mathbf{u})} \mathrm{div}\,(fI) \cdot \mathbf{w} \,\mathrm{d}x + \int_{\Omega(\mathbf{u})} \nabla f \cdot \mathbf{w} \,\mathrm{d}x.\end{aligned} \tag{6.12}$$

□

This result is specially adapted to our requirements. For more general results and an introduction to the area of shape calculus with application to partial differential equations, we refer to Simon [311] or [114, 313].

This theorem can directly be applied to calculate the Jacobian of the variational formulations. Equation (6.9) must be considered as a simple tool for evaluation of the derivatives. This formula however requires high regularity of the function f at the boundary. For example, we consider the variational formulation of Laplace equation

$$A(\mathbf{u})(\phi) = \int_{\Omega} \nabla\mathbf{u} \cdot \nabla\phi \,\mathrm{d}x.$$

Now assume that $\Omega = \Omega(\mathbf{u})$ as stated in Theorem 6.10. The variational formulation has a double dependency on $\mathbf{u}$, appearing as trial function itself and by the domain's dependency. Formula (6.9) gives

$$A'(\mathbf{u})(\mathbf{w}, \phi) = \int_{\Omega} \nabla\mathbf{w} \cdot \nabla\phi \,\mathrm{d}x + \int_{\partial\Omega} (\mathbf{n} \cdot \mathbf{w}) \nabla\mathbf{u} \cdot \nabla\phi \,\mathrm{d}o.$$

For this expression to be well-defined, we need traces of $\nabla \mathbf{u}$ and $\nabla \phi$. For H^1-functions, this regularity is not given. The crucial step in Theorem 6.10 is hidden in (6.12) using integration by parts. While the volume-formulation of the derivative is well-defined, the boundary integral formally requires higher regularity. See [311] for a discussion.

By the combination of Theorem 6.10 and Lemma 6.9, we can derive the complete Jacobian of the Fully Eulerian fluid-structure interaction problem.

Theorem 6.11 (Jacobian of the Fully Eulerian Formulation of Fluid-structure Interactions) *For the directional derivative of formulation (6.8) in* $\mathbf{U} = \{\mathbf{v}, \mathbf{u}, p\}$ *in direction of* $\mathbf{W} = \{\mathbf{z}, \mathbf{w}, q\}$ *it holds*

$$
\begin{aligned}
A'(\mathbf{U})(\mathbf{W}, \Phi) = & \left(\rho_f(\partial_t \mathbf{z} + \mathbf{z} \cdot \nabla \mathbf{v} + \mathbf{v} \cdot \nabla \mathbf{z}), \phi\right)_{\mathcal{F}(t)} \\
& + \left(\frac{d\boldsymbol{\sigma}_f}{d\mathbf{v}}(\mathbf{z}) + \frac{d\boldsymbol{\sigma}_f}{dp_f}(q_f), \nabla \phi\right)_{\mathcal{F}(t)} \\
& + \left(\frac{dJ_s}{d\mathbf{u}}(\mathbf{w})\hat{\rho}_s(\partial_t \mathbf{v} + \mathbf{v} \cdot \nabla \mathbf{v}) + J_s(\partial_t \mathbf{z} + \mathbf{z} \cdot \nabla \mathbf{v} + \mathbf{v} \cdot \nabla \mathbf{z}), \phi\right)_{\mathcal{S}(t)} \\
& + \left(\frac{d\boldsymbol{\sigma}_s}{d\mathbf{u}}(\mathbf{w}), \nabla \phi\right)_{\mathcal{S}(t)} + (\nabla \cdot \mathbf{z}, \xi_f)_{\mathcal{F}(t)} \\
& + \left(\partial_t \mathbf{w} + \mathbf{v} \cdot \mathbf{w} + \mathbf{z} \cdot \mathbf{u} - \mathbf{z}, \psi_s\right)_{\mathcal{S}(t)} + \left(\nabla \mathbf{w}, \nabla \psi_f\right)_{\mathcal{F}(t)} \\
& + \langle \rho_f(\partial_t \mathbf{v}_f + \mathbf{v}_f \cdot \nabla \mathbf{v}_f), (\mathbf{w}_f \cdot \mathbf{n}_f)\phi \rangle_{\mathcal{I}(t)} + \langle \boldsymbol{\sigma}_f, \nabla \phi (\mathbf{w}_f \cdot \mathbf{n}_f) \rangle_{\mathcal{I}(t)} \\
& + \langle \nabla \cdot \mathbf{v}_f, \xi_f (\mathbf{w}_f \cdot \mathbf{n}_f) \rangle_{\mathcal{I}(t)} + \langle J_s \hat{\rho}_s (\partial_t \mathbf{v}_s + \mathbf{v}_s \cdot \nabla \mathbf{v}_s), \phi (\mathbf{w}_s \cdot \mathbf{n}_s) \rangle_{\mathcal{I}(t)} \\
& + \langle \boldsymbol{\sigma}_s, \nabla \phi_s (\mathbf{w}_s \cdot \mathbf{n}_s) \rangle_{\mathcal{I}(t)} + \langle \partial_t \mathbf{u}_s + \mathbf{v}_s \cdot \nabla \mathbf{u}_s - \mathbf{v}_s, \psi_s (\mathbf{w}_s \cdot \mathbf{n}_s) \rangle_{\mathcal{I}(t)} \\
& + \langle \nabla \mathbf{w}_f, \nabla \psi_f (\mathbf{w}_f \cdot \mathbf{n}_f) \rangle_{\mathcal{I}(t)},
\end{aligned}
$$

where the directional derivatives of the deformation gradient, the stresses and the strains are defined in Lemma 6.9.

For the computations of the boundary terms, it must be considered, that the gradients of $\mathbf{v}$ and $\mathbf{u}$ are not continuous across $\mathcal{I}(t)$. Therefore, we denote the correct side by adding the subscripts "f" and "s" where necessary.

Remark 6.12 Including shape derivatives in the computation of the Jacobian significantly complicates the implementation work. In [126, 127] it is noted that computational approaches for linearization and also for sensitivity based optimization work well, if these shape derivatives are neglected. At the latest when optimization problems are considered, it will be necessary to include these terms, as they will be crucial for the determination of the adjoint information transport across the interface, see also Sect. 9.

6.5 Finite Elements for the Fully Eulerian Framework

The Fully Eulerian framework for fluid-structure interactions leads to an interface problem. The interface $\mathcal{I}(t)$ must be captured and across this interface, the solution $\{\mathbf{u}, \mathbf{v}\}$ suffers from a lack of accuracy. As has been discussed in Sect. 4.5, we must expect a breakdown in convergence rates, if we do not accurately treat the are around this interface.

The parametric finite element scheme proposed in Sect. 4.5 can directly be applied to this more complex coupled problem. As velocity and deformation are globally defined as continuous functions, no special adjustments are necessary. Only the coupling between velocity and pressure must be carefully considered. In [151], Frei discusses several alternatives to stabilize the inf-sup condition on meshes resulting from the parametric interface resolution. None of the techniques however is fully satisfactory. Instead, the definition and implementation of an inf-sup stable finite element pair remains an open topic.

Away from the moving interface $\mathcal{I}(t)$, standard finite element pairs can be used for the discretization of velocity, pressure and also for the deformation. To simplify a direct variational coupling of velocities and deformations across the interface, and to avoid local changes of basis functions, the same function spaces should be used within the fluid and the solid domain. For details, we refer to Sects. 4.3 and 5.3.

For further reading, we refer to the literature [151, 154] and also to Chap. 12 of this book.

6.6 Numerical Study

For validation of the Eulerian model, we first consider two simple fluid-structure interaction benchmarks, the *csm-1* problem and the *fsi-1* problem as proposed by Hron and Turek [199]. Both benchmark problems use the configuration as shown in Fig. 6.1, where an incompressible fluid flows around a circular obstacle and an elastic beam that is attached to this rigid obstacle. In the *csm-1* benchmark configuration the fluid is initially at rest and the beam undergoes a deformation caused by a gravity force. In the *fsi-1* benchmark problem no gravity force is

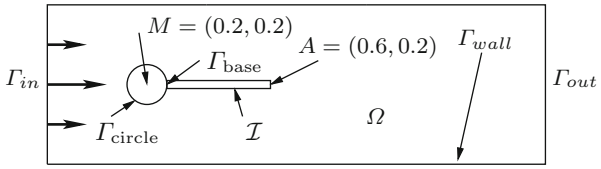

Fig. 6.1 Configuration of the *csm-1* and *fsi-1* benchmark problems as published by Hron and Turek [199]

acting, but the flow is driven by an inflow profile. Both problems have a stationary solution and highly accurate results for different functional values are available in literature [199, 201]. Finally, we describe a more challenging test case, where an elastic ball falls in an container filled with an incompressible fluid. The ball touches the bottom of the container and rebounces. Here we focus on modeling this collision of elastic structure with the domain's boundary.

6.6.1 Stationary Structure Benchmark Problem

In this first test case, a gravity force is acting on the elastic structure and causes a deflection, see Fig. 6.1. In the original benchmark configuration [199] $g_s = 2$ has been used, Wick [342] also published results for $g_s = 4$ yielding a larger deformation. To exploit the possibilities of very large deformation with the Eulerian approach, we add a further test case using $g_s = 8$. We measure the deformation $\mathbf{u}_s$ in the tip of the beam $A = (0.6, 0.2)$ in the stationary limit. In Table 6.1 we present the deflections in this measurement point on different meshes with decreasing mesh sizes under three different gravity forces. For comparison, we indicate the reference values are stated in [199, 201] and [342, 344]. The complete set of parameters used in this configuration is:

$$\begin{aligned} &\rho_f = \hat{\rho}_s = 10^3, \quad \nu_f = 10^{-3}, \quad \mu_s = 5 \cdot 10^5, \\ &\lambda_2 = 2 \cdot 10^6, \quad \mathbf{f}_s = -g_s J_s \hat{\rho}_s \chi_s. \end{aligned} \tag{6.13}$$

The Fully Eulerian method yields accurate values which are very close to the reference values cited from the literature. Further, the Eulerian framework is able to increase the gravity force up to a point ($g_s = 8$) where the beam touches the rigid bottom of the flow-channel, see Fig. 6.2. Here, no results for comparison are available in the literature.

Table 6.1 Results for the CSM-1 benchmark problem using increasing volume forces

	$g_s = 2$		$g_s = 4$		$g_s = 8$	
Mesh size	$u^x(A)$	$u^y(A)$	$u^x(A)$	$u^y(A)$	$u^x(A)$	$u^y(A)$
$h_{\min} \approx 0.008$	6.372	61.84	21.22	114.54	59.846	189.74
$h_{\min} \approx 0.004$	7.116	64.70	25.02	121.25	65.760	192.03
$h_{\min} \approx 0.002$	7.149	66.07	25.10	122.16	66.857	192.35
Hron and Turek [199]	7.187	66.10	n/a		n/a	
Wick [342, 344]	7.150	64.90	25.33	122.30	n/a	

Functional values on a sequence of meshes. Comparison to reference values taken from the literature using the ALE framework

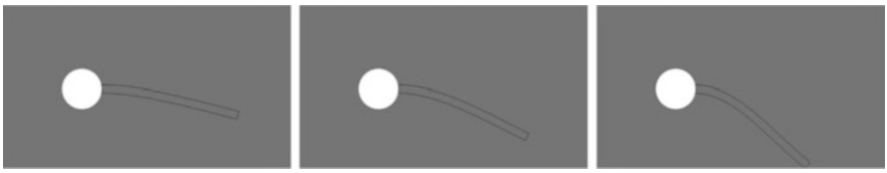

Fig. 6.2 Configuration of the *csm-1* benchmark problem and modifications with larger gravity force. *Left* $g_s = -2$, *middle* $g_s = -4$ and *right* $g_s = -8$

6.6.2 Stationary Fluid-structure Interaction Problem

As a second test case of the benchmark-suite published by Hron & Turek we refer to the *fsi-1* problem. The flow is driven by a parabolic inflow profile on the boundary Γ_{in}:

$$\mathbf{v}_{\text{in}} = \frac{y(H-y)}{4H^2} v_{\max}, \quad H = 0.41, \quad \mathbf{v}_{\max} = 0.3.$$

Due to a slight unbalance in the configuration (see Fig. 6.1) the elastic beam undergoes a small deflection. Apart from this modification, the material constants are taken as described in (6.13). Besides measuring the deflection of the beam, drag- and lift-values of the obstacle (rigid circle & beam) where to be estimated. Let $\Gamma_{\text{obs}} := \mathcal{I} \cup \Gamma_{\text{circle}} \setminus \Gamma_{\text{base}}$ be the complete outer boundary of the obstacle. Here, we consider the drag-value:

$$J_{\text{drag}} = \int_{\Gamma_{\text{obs}}} \mathbf{n}_f \boldsymbol{\sigma}_f \mathbf{e}_x \, \mathrm{d}s.$$

Evaluation of these integrals is accomplished by rewriting the boundary integrals over the moving interface $\mathcal{I}(t)$ into integrals over the fixed boundary around the rigid circle, followed by a reformulation into volume integrals. Finally, we can compute the drag force as a residual evaluation. We first modify the functionals by using the dynamic coupling condition and inserting zero:

$$\begin{aligned} J_{\text{drag}} &= \int_{\Gamma_{\text{circle}} \setminus \Gamma_{\text{base}}} \mathbf{n}_f \boldsymbol{\sigma}_f \mathbf{e}_x \, \mathrm{d}s + \int_{\mathcal{I}} \underbrace{\mathbf{n}_f \boldsymbol{\sigma}_f}_{=-\mathbf{n}_s \boldsymbol{\sigma}_s} \mathbf{e}_x \, \mathrm{d}s \pm \int_{\Gamma_{\text{base}}} \mathbf{n}_s \boldsymbol{\sigma}_s \mathbf{e}_x \, \mathrm{d}s \\ &= \int_{\Gamma_{\text{circle}} \setminus \Gamma_{\text{base}}} \mathbf{n}_f \boldsymbol{\sigma}_f \mathbf{e}_x \, \mathrm{d}s + \int_{\Gamma_{\text{base}}} \mathbf{n}_s \boldsymbol{\sigma}_s \mathbf{e}_x \, \mathrm{d}s - \int_{\partial \Omega_s} \mathbf{n}_s \boldsymbol{\sigma}_s \mathbf{e}_x \, \mathrm{d}s. \end{aligned}$$

In the stationary limit (and in the absence of external forces) it holds for the exact solution $\int_{\partial \Omega_s} \mathbf{n}\boldsymbol{\sigma} \, \mathrm{d}s = -\int_{\Omega_s} \operatorname{div} \boldsymbol{\sigma}_s \, \mathrm{d}x = 0$ and hence:

$$J_{\text{drag}} = \int_{\Gamma_{\text{circle}}} \mathbf{n}\boldsymbol{\sigma} e_1 \, \mathrm{d}s,$$

where by $\mathbf{n}$ we denote the outward facing normal vector (whether in Ω_f or Ω_s) and by $\boldsymbol{\sigma}$ the corresponding acting tensor. Evaluation of this boundary integral is straightforward, since the boundary Γ_{circle} is fixed, even in the Eulerian setting. The accuracy of this functional evaluation can be further enhanced by expressing it in terms of variational residuals,the *Babuška-Miller-Trick* [16, 88, 280]. In Table 6.2 we gather the drag-value obtained with the Eulerian approach. For evaluation of the functional we consider both the boundary integrals as well as the reformulation into residual terms. A good reference value $J_{\text{drag}} = 14.2940 \pm 10^{-5}$ is available in the literature [201, 280]. In Fig. 6.3 we show the error slopes of the drag approximation. Here we observe linear order of convergence (in the mesh-size h) for the boundary integral and quadratic convergence for the residual reformulation. Using piecewise linear finite elements one would expect (at least for a pure incompressible flow problem) the double order of convergence. Order reduction will take place due to the limited discretization accuracy close at the elements that are cut by the moving interface. Remedy could be found by using local mesh adaptation close to the interface or considering the extended finite element method [95] for better accuracy in the interface region. See Chap. 8 for details on adaptivity and Sect. 4.5 for techniques to discretize interface problems. Frei [151] showed results for the

Table 6.2 *fsi-1* benchmark results

Mesh-size	dof's	Boundary	Variational
0.1	53,450	15.1052	14.9004
0.05	176,790	15.2333	14.5971
0.025	640,490	14.7836	14.4062
0.0125	2,466,390	14.5118	14.3280

Drag-coefficient $J_{\text{drag}}(U_h)$ evaluates as boundary integral and reformulated as residual expression. The reference value taken from literature is given by $J_{\text{drag}} = 14.2940 \pm 10^{-5}$

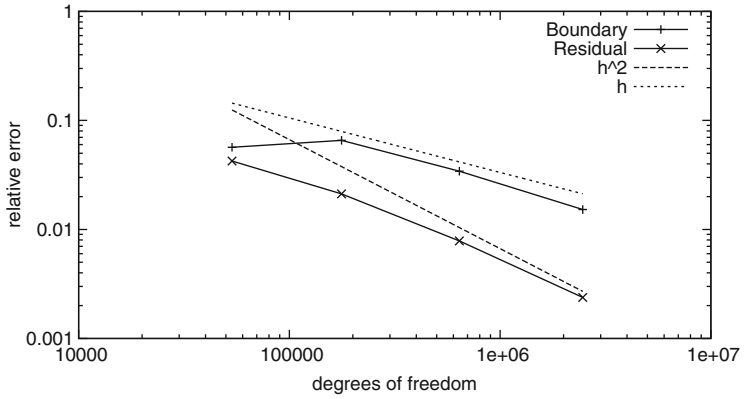

Fig. 6.3 Convergence of the drag-approximation with the Eulerian coordinate framework. Evaluated as boundary integral (linear convergence) and as residual term (quadratic convergence)

Fully Eulerian approach that do not suffer these order reductions, as accurate and efficient numerical schemes are used. Once more, we also refer to Chap. 12.

For a study of the time-dependent version fsi-3 of the benchmark problem, we refer to the results shown by Frei [151]. Given an adequate handling of the interface discretization with the locally modified scheme presented in Sect. 4.5 and accurate time stepping on moving interfaces as presented in Sect. 4.6, the Fully Eulerian model is able to reproduce the reference results from [330].

6.6.3 Contact Problem

Finally, we model the "free fall" of an elastic ball Ω_s with radius $r_{\text{ball}} = 0.4$ in a container $\Omega = (-1, 1)^2$ filled with a viscous fluid Ω_f. The container is closed at the bottom boundary $\Gamma_{\text{bot}} = \partial\Omega_{y=-1}$ but open at the top and the sides. Here, by open we refer to the "do-nothing" boundary condition

$$\nu \partial_n \mathbf{v} - p\mathbf{n} = 0,$$

which allows free in- and outflow of the fluid, see [188].

Figure 6.4 shows the configuration of this test case. At time $t = 0$, the midpoint of the ball is at $x_0 = (0, 0)$. Since gravity is the only acting force on the solid, the ball will accelerate and fall to the bottom

$$\Gamma_{\text{bot}} = \{(x, -1),\ x \in (-1, 1)\}.$$

At this rigid wall with homogenous Dirichlet condition $\mathbf{v}_f = 0$, the ball stops and due to elasticity it will bounce off again. The parameters used for this test case are given by

$$\begin{aligned} &\rho_f = 10^3, \quad \hat{\rho}_s = 10^3, \quad \nu_f = 10^{-2} \\ &\mu_s = 10^4, \quad \lambda_s = 4 \cdot 10^4, \quad \mathbf{f} = -J_s \hat{\rho}_s \chi_s. \end{aligned} \tag{6.14}$$

To get a closer look at the processes during "contact", we show in Fig. 6.5 a zoom into the are close to the lower boundary. We note that these computations have been done with a standard finite element basis, without using the parametric approach described in Sect. 4.5. Figure 6.5 shows simulation results for the time, where the structure enters the last layer of elements at the boundary, the time, where the ball gets closest to the boundary (here, a significant deformation of the structure is visible) and at a time, where the ball starts to release and finally, a snap-shot of the simulation, where the ball is completely detached. The Fully Eulerian formulation does not model real contact, as solid and boundary never touch.

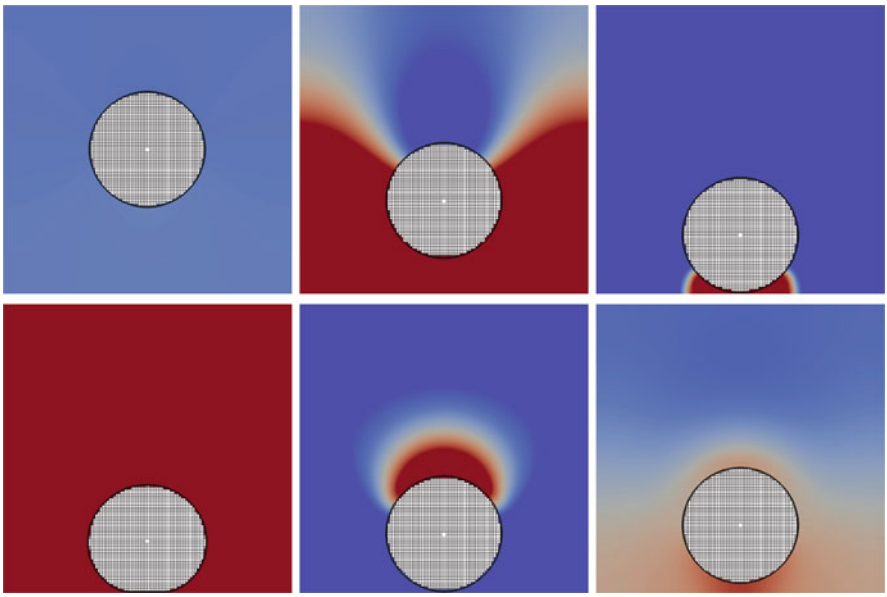

Fig. 6.4 Falling ball bouncing of the bottom wall. Snapshots of the solution at times $t = 0$, $t = 0.71$, $t = 0.96$ (first contact), $t = 1.035$ (biggest deformation), $t = 1.125$ (breaking contact) and $t = 1.38$ (highest bounce-off)

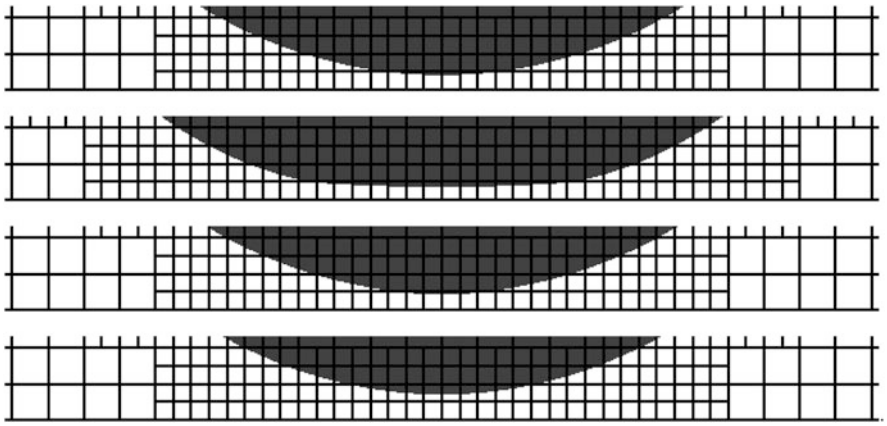

Fig. 6.5 Close ups of the contact problem. *From top to bottom*: simulation at times, where the ball first gets into the last layer of elements at the contact boundary, shortest distance to the boundary, beginning of release and full detachment

Remark 6.13 (Contact in Fluid-structure Interactions) It is a widely discussed question if contact in the case of the coupled dynamics of the incompressible Navier-Stokes equations and a solid body is possible at all. First of all, physical observation, i.e. a steel ball touching the ground, tells us that contact is established. On the other

hand, theoretical results, considering the fall of an rigid body with smooth boundary in an incompressible fluid show that contact (in the usual variational sense) will not be reached in finite time, see e.g. [115, 136, 189, 190, 241]. To the best knowledge of the author, no theoretical analysis has been done for collision problems of elastic structures in viscous fluids.

For the interaction of an elastic solid with smooth boundaries and a viscous fluid, one hypothesis is that a finite layer of fluid will always remain. In numerical simulations based on strong local adaptivity, this could however not be assured (neither disproved) so far.

From a modeling point of view, the use of the incompressible Navier-Stokes equations is questionable for such limiting applications. First of all, also water will not behave strictly incompressible, if very large forces act on a very thin film. Secondly, the continuum hypothesis must be queried in the transmission to contact.

To shed further light on the mechanism acting at "close contact", we consider the following functional outputs measuring stresses in fluid and solid: We measure the wall stress acting on the lower boundary and the elastic stress stored in the solid:

$$J_{\text{fluid}}(U) = \int_{\Gamma_{\text{bot}}} \boldsymbol{\sigma}_f \mathbf{n}_f \cdot \mathbf{n}_f \, \mathrm{d}o, \quad J_{\text{solid}}(U) = \left(\int_{\mathcal{S}(t)} \boldsymbol{\sigma}_s : \boldsymbol{\sigma}_s \, \mathrm{d}x \right)^{\frac{1}{2}}. \tag{6.15}$$

The results—together with the distance of the ball from the lower boundary—are shown in Fig. 6.6. Forces are transmitted through the remaining small liquid film and elastic energy is stored in the solid.

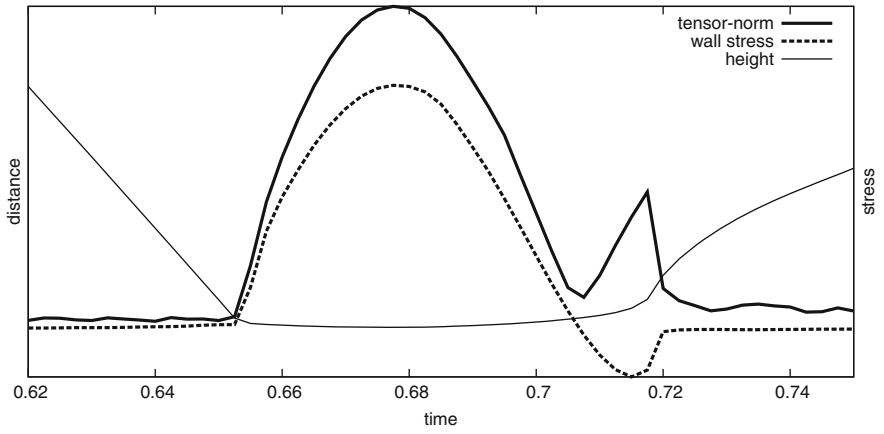

Fig. 6.6 Wall stress on the lower boundary and stresses in the solid during "contact"

Table 6.3 Error in mass conservation for the falling ball

h/k	0.0100	0.0050	0.0025
2^{-5}	$2.68 \cdot 10^{-3}$	$2.66 \cdot 10^{-3}$	$2.69 \cdot 10^{-3}$
2^{-6}	$7.82 \cdot 10^{-4}$	$6.95 \cdot 10^{-4}$	$6.72 \cdot 10^{-4}$
2^{-7}	$2.63 \cdot 10^{-4}$	$1.92 \cdot 10^{-4}$	$1.68 \cdot 10^{-4}$

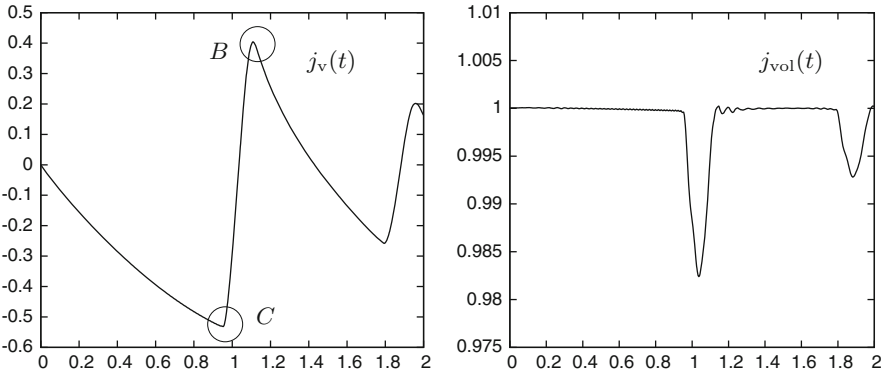

Fig. 6.7 Falling ball: functionals as plot over time. *Left*: solid's average velocity. *Right*: solid's relative volume. The two turning points of the velocity for contact (C) and maximum bounce-off (B) are indicated in the middle plot

Finally, to measure the quality of the approximation we indicate some further output functionals of the solution. First, as the Eulerian model does not have exact conservation properties, we analyze the solid's mass, measured as

$$J_{\text{mass}}(U) = \int_{\mathcal{S}(t)} J_s \hat{\rho}_s^0 \, \mathrm{d}x.$$

In Table 6.3 we show the error in mass conservation

$$\| j_{\text{mass}}(t) - \hat{\rho}_s \pi r_{\text{ball}}^2 \|_{L^2([0,2])},$$

depending on the accuracy of the spatial and temporal discretization. The time-interval $I = [0, 2]$ is so large that the ball hits the bottom boundary twice. We observe $O(h^2)$ convergence, even if we did not use the modified finite element approach described in Sect. 4.5. The time-discretization parameter k appears to be too small to have a substantial influence on the accuracy. strictly guarantee this conservation.

In Fig. 6.7 we show two further output functionals measuring the average vertical velocity of the ball and the volume of ball, both as functions over time:

$$J_{\mathbf{v}}(t) := \int_{\Omega_s(t)} \mathbf{v}_s^y(t) \, \mathrm{d}x, \quad J_{\text{vol}}(t) := \int_{\Omega_s(t)} 1 \, \mathrm{d}x. \tag{6.16}$$

Table 6.4 Left: maximum (negative) velocity reached in free fall. Right: maximum average velocity after bounce-off

h/k	0.0100	0.0050	0.0025
2^{-5}	−0.4977	−0.4990	−0.5006
2^{-6}	−0.5248	−0.5286	−0.5298
2^{-7}	−0.5402	−0.5311	−0.5315

h/k	0.0100	0.0050	0.0025
2^{-5}	0.320	0.348	0.365
2^{-6}	0.318	0.369	0.396
2^{-7}	0.357	0.388	0.404

Calculations on three different spatial and temporal meshes

Note that mass should be conserved, the volume of the elastic obstacle however is subject to change, as $\nu_s = 0.4$, compare (6.14).

Figure 6.7 shows the progress of the functionals (6.16) as function over time. The left sketch shows the average velocity. Here, acceleration by gravity and acceleration due to bounce of are clearly visible. The boundary of height is smaller (due to viscous damping). The right sketch shows the volume of the ball. Due to the compression at impact-time, the volume gets reduced during the contact. Reduction of volume is possible, since the flow-container is open on the upper, left and right boundaries.

Finally, in Table 6.4 we indicate the maximum (negative) velocity that is reached at the time of first contact $t_C \approx 0.952$, as well as the maximum velocity that is reached after the first bounce-off $t_B \approx 1.105$, see Fig. 6.7. Computations are done using three different temporal and spatial discretization parameters h and k. All meshes are uniform in space and time. While the time step has only a very small influence on the functional values we observe convergence under mesh-refinement.

The problem of an elastic ball, falling in a viscous fluid has been revisited by Frei [151]. Here, detailed studies including contact modeling are given. In particular it is found that for certain configurations, a minimal distance between ball and bottom of the flow container can be identified in numerical simulation, such that no real contact will take place at first touch-down. A numerical study with accurate interface discretization techniques is found in the guest article of Frei, Chap. 12 of this book.